Emergence of Orchestrated and Dynamic Metabolism of *Saccharomyces cerevisiae*

Viviana Nguyen[1,3,7], Yifei Li[2,3,7], and Ting Lu[2,3,4,5,6,8]

[1]Department of Physics, [2]Center for Biophysics and Quantitative Biology, [3]Center for Advanced Bioenergy and Bioproducts Innovation, [4]Department of Bioengineering, and [5]Carl R Woese Institute for Genomic Biology, [6]National Center for Supercomputing Applications, University of Illinois Urbana-Champaign, Urbana, IL 61801, USA

[7]These authors contributed equally to the work.

[8]Lead Contact: Ting Lu (Email: luting@illinois.edu)

Keywords:

Systems biology; microbial metabolism; Saccharomyces cerevisiae; mathematical modeling; complexity and emergence

Summary

Microbial metabolism is a fundamental cellular process that is rooted in molecular biochemical events and responsible for the emergence of cellular properties. While molecular details of individual reactions have been greatly elucidated, it is not well understood quantitatively how these reactions orchestrate and alternate and how these molecular events produce collective cellular behaviors. Here we developed a coarse-grained, systems and dynamic mathematical framework, which integrates metabolic reactions with signaling and gene regulation, to dissect the emergence of metabolic traits of *Saccharomyces cerevisiae*. The framework mechanistically captures a set of characteristic cellular behaviors, including the Crabtree effect, the diauxic shift, diauxic lag time, and differential growth under nutrient-altered environments. It also allows modular expansion for zooming in on specific pathways for detailed metabolic profiles. This study uncovers a mechanistic, causal relationship between molecular coordination and emergent cellular properties, providing insights into quantitative microbial physiology and metabolic engineering practice.

Introduction

Metabolism dictates the growth, adaptation, and functioning of microorganisms. It characterized by extraordinary complexity that is rooted in three key factors. First, microbial metabolism engages a remarkable number of molecular species. For example, *S. cerevisiae* metabolism involves 16,042 metabolites and 919 enzymes[1]. Second, metabolic reactions are intrinsically coupled with signaling and gene regulation. For *S. cerevisiae*, glucose metabolism is monitored by signal transduction centered around the regulators PKA and SNF1, which control the catalytic activity and transcription of enzymes for glycolysis, gluconeogenesis, and respiration[2-5]. Third, metabolism is highly dynamic, constantly responding to changing intracellular and extracellular environments. *S. cerevisiae* actively modulates its protein abundance and metabolic fluxes when external glucose shifts[2-5] or intracellular amino acids fluctuate[6].

Because of its complexity, *S. cerevisiae* metabolism exhibits emergent properties that arise from interactions between its metabolic, signaling, and gene regulatory components. For instance, during aerobic growth on glucose, accelerated glycolysis yields excessive pyruvate, which exceeds the processing capacity of respiration and results in ethanol fermentation, a phenomenon called the Crabtree effect[7]. Another example of emergence is the diauxic shift. Upon glucose depletion in aerobic glucose batch cultures, *S. cerevisiae* utilizes SNF1-mediated signaling to transition from ethanol production to assimilation by dynamically reprogramming its enzyme abundance[8-10].

Understanding metabolism is important because it underlies the generation of energy and building blocks for various cellular events. Dissecting that of *S. cerevisiae* is particularly invaluable because this organism is extensively used in the food and beverage industry for fermentation[11] and in metabolic engineering as a prominent factory for sustainable chemical production[11,12]. Additionally, *S. cerevisiae* serves as a powerful model system for decoding the fundamental laws of organization for higher eukaryotes[13] and as a useful testbed for studying human diseases[14-16] and drug testing[17].

Substantial progress has been made towards the understanding and engineering of *S. cerevisiae* metabolism. Mathematical modeling has been a particularly valuable tool for systematically describing large quantities of molecular species and integrating their intricate interactions. Two important classes of models that have been developed are detailed kinetic models[18-21] and genome-scale models[22-24]. The former typically employs mechanistic descriptions for individual or small sets of pathways whereas the latter aims to exhaust all known metabolic

details for a comprehensive illustration of metabolism. While offering certain advantages, each of these model classes has inherent limitations. Detailed kinetic models often underestimate the impact of the system-level integration intrinsic to microbial metabolism. They are also challenged by the lack of molecular reaction details and uncertain parameters[25]. Genome-scale models assume quasi-steady-state conditions and therefore offer limited information on system dynamics. Moreover, the complexity of genome-scale models complicates drawing biophysical insights. Consequently, kinetic and genome-scale models offer limited quantitative information on how metabolic reactions interact with signaling and gene regulatory events and on how the integration of metabolic processes gives rise to collective cellular behaviors.

Here, we propose a coarse-grained, systems, and dynamic model to quantitatively unravel the emergent traits of *S. cerevisiae* metabolism. Coarse-graining is a mathematical scheme that groups variables with similar functions and patterns to reduce system complexity[26]. Recent experiments suggested that metabolites and proteins located within the same pathway in *S. cerevisiae* share similar behaviors and therefore can be treated as similar variables in a coarse grained procedure. For example, during the glucose-to-ethanol diauxic shift, the concentrations of metabolites in upper glycolysis decline but those of lower glycolysis and the TCA cycle increase[9,27]; concurrently, the abundances of ribosomal proteins drop while those of the enzymes for respiration and gluconeogenesis rise[10]. By reducing complexity, coarse graining allows us to describe metabolism in both a systems fashion that integrates metabolic reactions, signaling, and gene regulation and a dynamic manner that considers temporal changes of key molecular, cellular, and environmental variables. Our model simulates the metabolic characteristics of *S. cerevisiae* by capturing the Crabtree effect and diauxic shift, tracing the origin of lag time during a nutrient shift, and accounting for differential growth in rich and minimal media. Additionally, our modular model can be easily expanded by zooming in on specific pathways, such as glycolysis, for a more detailed illustration of metabolic patterns. Together, our results provide a quantitative framework that yields characteristic metabolic traits of *S. cerevisiae*, advancing the basic understanding of its metabolism.

Results

A coarse-grained, systems, and dynamic model. To manage the complexity of *S. cerevisiae* metabolism, we used a modular model design that decomposes the system into three parts, namely

metabolic reactions, signaling, and gene regulation (Fig. 1a). Each module was coarse-grained and characterized individually before assembly into one integrated framework (Supplementary Method 1.1).

The metabolic reactions module contains a simplified description of the central carbon metabolism (Fig. 1b, Supplementary Method 1.3). Fluxes were considered from carbon substrates (glucose or ethanol) to metabolic precursors; then to ethanol, ATP, and amino acids; and, finally, to proteins. Intermediates within the central carbon metabolism were lumped into a single metabolite representing the growth-limiting precursor. The associated precursor biosynthesis and utilization reactions were collapsed into single steps (Supplementary Method 1.3.1). For example, reactions for glucose utilization, including glucose uptake and glycolysis, were coarse-grained into the glucose-to-precursor reaction. Reactions for ethanol utilization, including ethanol uptake, the glyoxylate cycle, and gluconeogenesis, were condensed into the conversion of ethanol to precursor. Ethanol fermentation and respiration from pyruvate were encapsulated in the reactions from precursor to ethanol and precursor to ATP, respectively. Amino acids were also binned into one effective molecule representing the growth-limiting amino acid, and its synthesis and uptake were modeled as single reactions from precursor or from the extracellular growth-limiting amino acid (Supplementary Method 1.3.2). Each of these reactions is catalyzed by a corresponding coarse-grained enzyme (Fig. 1b, green squares) including that for glucose utilization (E_{gy}), respiration (E_{mt}), fermentation (E_{fe}), amino acid biosynthesis (E_{as}), ethanol utilization (E_{gn}), and amino acid uptake (E_{at}). The reactions may be subject to dynamic regulation via metabolite feedforward and feedback controls (Fig. 1b, gray arrows) or global signaling-mediated regulation (Fig. 1b, tan arrows).

The signaling network was constructed by considering how cells transmit metabolic information to direct cellular resource partitioning (Supplementary Method 1.4). *S. cerevisiae* leverages multiple signaling routes to regulate resource partitioning globally, including those that monitor the extracellular glucose concentration, such as PKA and SNF1[2-5], and the intracellular amino acid concentration, such as TORC1 and GCN2[3,5,6]. When glucose is abundant, PKA promotes the synthesis of ribosomal and ribosome-affiliated proteins[2-5] and the activity of glycolytic enzymes[28,29]. When the glucose is absent, SNF1 promotes the synthesis of enzymes for ethanol utilization and respiration[2-5] and inhibits that of amino acid biosynthesis enzymes[30]. Because PKA and SNF1 function in a coupled but opposite fashion, we coarse-grained these

molecules, along with other glucose-responsive regulators, into a single effective signaling molecule SNF1 that mediates glucose signaling (Supplementary Methods 1.4.1). Additionally, recent experiments suggested that the activities of PKA and SNF1 are controlled by an intracellular glucose uptake flux sensor[31,32]. In our model, precursor fulfills the role of the glucose uptake sensor, so the activity of the coarse-grained SNF1 molecule is inhibited by precursor (Supplementary Method 1.4.2). Meanwhile, TORC1 and GCN2 modulate the production of amino acid biosynthesis enzymes concurrently with the activity and abundance of ribosomes to maintain amino acid homeostasis[3,6]. Here, the TORC1 and GCN2 cascades, along with other associated signaling pathways, were coarse-grained into a single species TORC1 (Supplementary Method 1.4.3) to account for dynamic sensing of amino acid availability (Supplementary Method 1.4.4).

The gene regulation module describes protein synthesis (Supplementary Method 1.5). Similar to the pioneering work on *E. coli*[33,34], the entire yeast proteome was coarse-grained into three sectors including ribosomal and ribosome-affiliated proteins for cytosolic translation (R), enzymes for metabolic conversions (E), and all other proteins for housekeeping (Z) (Supplementary Method 1.5.1 and Supplementary Table 1). The E sector was further divided into six subsectors, one for each of the coarse-grained conversions detailed in the metabolic reactions module. Each coarse-grained protein is assigned an effective mRNA as a template for transcription, which is either constitutive or regulated by SNF1 or TORC1 (Supplementary Method 1.5.3). Notably, we assumed that transcription of E_{gy} and E_{at} are unregulated because each is comprised of plasma membrane transporters whose expressions may vary oppositely depending on their regulatory details[35,36] (Supplementary Fig. 1). Additionally, ribosomes were classified into three forms, namely free ribosomes, translating ribosomes bound with charged tRNA and elongating the peptide chain, and stalled ribosomes attached to mRNA but bound by uncharged tRNA and incapable of peptide chain elongation. The processes of transcription and translation were condensed into a single step to describe the synthesis of each coarse-grained protein.

The three modules were subsequently combined into an integrated framework by connecting their inputs and outputs. Specifically, the metabolic module outputs metabolite concentrations, which are inputs for the signaling module. The signaling module then yields the concentration of active global regulators, which in turn act as inputs for both the metabolic reactions module to regulate enzyme activity and the gene regulation module to tune protein synthesis. The outputted proteins from the gene regulation module are also additional inputs for

metabolic reactions. Model parameters (Supplementary Table 2) were obtained either from literature or through data fitting (Supplementary Method 2 and Supplementary Fig. 2) and were analyzed using both local and global sensitivity analyses to ensure their robustness (Supplementary Method 2.8 and Supplementary Figs. 3 and 4).

The model captures the Crabtree effect. To illustrate the utility of the model, we showed that it predicts the Crabtree effect in both glucose-limited chemostat cultivations (Fig. 2) and glucose batch fermentations (Fig. 3). Using simulation settings that mimic the experimental conditions[37-40] (Supplementary Table 3 and Supplementary Method 4.1), we first examined the growth of wildtype *S. cerevisiae* in a glucose-limited chemostat environment. Fig. 2a-l compares simulated (lines) and experimental (symbols) results for key variables at various dilution rates. Here, ethanol production (Fig. 2c) shows a phase transition from a null value to a linear increase when the dilution rate exceeds a threshold (i.e., the critical dilution rate), indicating the onset of the Crabtree effect. The glucose uptake rate (Fig. 2a) and the cell population (Fig. 2f) also exhibit biphasic patterns. Concurrently, the precursor concentration (Fig. 2b) rises with increasing dilution rate, and the intracellular amino acid concentration (Fig. 2d) initially increases before leveling off. The active SNF1 and TORC1 concentrations mirror the precursor and intracellular amino acid concentrations, respectively (Supplementary Fig. 5). Regarding the coarse-grained enzyme concentrations, some remain relatively constant (Fig. 2g,h and Supplementary Fig. 6), two are initially constant but then begin to monotonically decrease before the dilution rate reaches the critical dilution rate (Fig. 2i,j), and one is initially constant but then monotonically increases (Fig. 2k). These varied patterns across the metabolic, signaling, and gene regulatory variables as well as the appearance of the Crabtree effect above the critical dilution rate demonstrate the systems nature of *S. cerevisiae* metabolism; that is, metabolic events, signal transduction, and gene regulation are intrinsically coupled, and their simultaneous orchestration generates interesting cellular behaviors.

One major unresolved issue concerns the origin of the Crabtree effect. Earlier efforts to model metabolism using flux balance analysis were unable to reproduce overflow metabolism until constraints were added[41-45], indicating that other biological factors must be considered in addition to flux optimization. Recently, resource allocation has been used to explain overflow metabolism[46]. Resources, including amino acids and protein synthesis machinery, are limited, so

increasing the production of one protein comes at the expense of another. Although fermentation produces less ATP per glucose molecule than respiration, it requires fewer resources. There, from the resource allocation perspective, overflow metabolism occurs when carbon is not limiting because more resources can be channeled towards ribosome production to support faster growth[47]. Because resource allocation is an intrinsic property of this model, we further expand on this idea and present the emergence of the Crabtree effect from a systems perspective.

Analysis of the behaviors of the R, E, and Z sectors provides insight on the high-level patterns of proteome partitioning underlying the Crabtree effect. In contrast with the enzyme subsectors exhibiting diverse patterns (Fig. 2g-k), the R, E, and Z sectors all show linear patterns (Fig. 2l). Specifically, the R sector augments gradually with increasing dilution rate whereas the E and Z sectors decrease. In chemostats, the specific growth rate of cells equals the dilution rate; therefore, the R concentration must increase with increasing dilution rates to confer a larger translational capacity that permits faster growth. Because protein synthesis machinery is shared, any increase in R must be met with an equal decrease in E and Z. Consequently, ATP production from respiration is reduced due to the repressed E_{mt} synthesis (Fig. 2j). This loss in ATP is offset by an increase in ATP production from the enhanced glucose-to-precursor flux (J_{gy}) (Fig. 2a). The precursor concentration also rises (Fig. 2b), increasing the substrate availability for J_{as} and J_{mt}. Quantitatively, J_{mt} and J_{as} may decrease or increase with dilution rate, as seen in different experiments[]. However, the J_{gy} influx augments much quicker, particularly above the critical dilution rate, resulting in the overflow of ethanol (Supplementary Fig. 7). This fine tuning of the proteome is possible because of SNF1 signaling, and this result suggests that the growth law developed in *E. coli*[33,34] is translatable to the description of cellular growth in yeast.

Consistent with recent experimental evidence suggesting that the substrate uptake rate is a key variable that controls the appearance of the Crabtree effect[49] (Supplementary Fig. 8), our model shows that decreasing the glucose uptake rate reduces, or even eliminates, ethanol overflow. We compared our simulation with experimental data from literature[50] for wild type *S. cerevisiae* and three hexose transporter mutants (one solely expressing HXT1, one only expressing HXT7, and an HXT1 and HXT7 recombinant strain (TM6)). Indeed, compared to the wild type, the HXT1 mutant consumed glucose slower and produced less ethanol whereas the HXT7 and TM6 mutants saw further reductions in glucose consumption and did not produce ethanol even though glucose was abundant (Fig. 2n-q). This reduced ethanol production is due to two compounding factors.

First, decreasing glucose uptake lowers the precursor concentration (Supplementary Fig. 9a). Because the affinity of E_{fe} for precursor is lower than that of E_{mt} (Supplementary Table 2), reducing the precursor concentration is sufficient to drive the flux from ethanol to ATP production. Second, increasing SNF1 activity promotes E_{mt} synthesis, and increased E_{mt} abundance raises the maximum J_{mt} flux (Supplementary Fig. 9b-d). Therefore, for ethanol overflow to occur, a higher precursor concentration is required to overcome the increased J_{mt} capacity. This application of our framework further illustrates that the Crabtree effect can be understood by considering the interactions between the metabolic reactions, signaling, and gene regulatory components of metabolism.

Diauxic growth during batch fermentations. Previous studies have shown that the temporal shifts seen in the metabolic reactions, signal transduction, and protein abundances during the diauxic shift are coordinated[9,10,51]; however, these studies often focused on only one or two of these parts[9,10,27,52] and were therefore incomplete in terms providing a comprehensive understanding of all three aspects. To create a complete picture of the temporal behaviors of the metabolic, signaling, and gene regulatory variables of wild type *S. cerevisiae* before, during, and after the diauxic shift (Fig. 3, circles), we pieced together four different sets of experimental data from glucose batch fermentations[9,10,27,52] (Supplementary Table 3). In parallel, we employed our integrated mathematical modeling framework to dissect the underlying behavior (Supplementary Method 4.2). As expected, during glucose consumption (Fig. 3a), there is continuous ethanol production (Fig. 3c). Additionally, during this phase, the concentrations of active SNF1 and TORC1 (Supplementary Fig. 10) are constant, which result in constant protein concentrations (Fig. 3g-l). When glucose is nearly depleted, there are significant reductions in the precursor (Fig. 3b) and intracellular amino acid (Fig. 3d) concentrations. The dramatic changes in these metabolite concentrations cause the active SNF1 and TORC1 concentrations to shift rapidly (Supplementary Fig. 10) to initiate proteome remodeling and prepare for ethanol assimilation. Specifically, the subset of the proteome that is remodeled includes E_{gn} (Fig. 3i, increases), E_{mt} (Fig. 3j, increases), E_{as} (Fig. 3k, decreases), and R (Fig. 3l, decreases). The concentrations of the other proteins remain largely constant (Fig. 3g,h and Supplementary Fig. 11). Following glucose depletion, cells consume the secreted ethanol (Fig. 3c) to begin another phase of growth (Fig. 3f). In contrast with the fast changes in the activities of the signaling molecules, the proteome changes slowly and is

continuously modulated throughout the duration of the diauxic shift and the ethanol utilization phase (Fig. 3g-l).

We further elaborate on the temporal behaviors of the high-level R, E, and Z proteome partitioning during the diauxic shift. Because enzymes essential for ethanol utilization, including E_{gn} and E_{mt}, are expressed at low levels during the glucose consumption phase (Fig. 3i,j), the concentration of the E sector must increase during the diauxic shift for there to be any ethanol consumption later. Because resources are limited, this increase in the E concentration must be accompanied by a reduction in the R concentration (Fig. 3l). These adjustments are made by SNF1, which represses synthesis of the R proteins while promoting that of E_{gn} and E_{mt}. These results confirm that the diauxic shift is a complex metabolic process involving continuous, coordinated shifts of metabolic reactions, signaling, and gene expression.

Lag time links to reallocation of cellular resources. One prominent feature of the diauxic shift is the temporary period of slow growth, the lag phase, that cells may experience between depleting glucose and resuming growth on ethanol (Fig. 3f). During this period, the proteome is being remodeled to prepare for ethanol assimilation[9,10]. The lag phase is not unique to the diauxic shift and occurs whenever cells adapt to new environments, such as during nutrient shifts[53]. Interestingly, a recent study analyzing a maltose-glucose-maltose shift experiment showed that past exposure to maltose decreases the lag time after the glucose-to-maltose shift[54] (Fig. 4d,e). We sought to understand how adaptations in signaling and gene regulation contribute to this effect. Because our model is characterized only for glucose and ethanol utilization, we simulated an ethanol-glucose-ethanol nutrient shift experiment (Fig. 4a) and tested if the result still applied. Cells pre-grown on ethanol were first transferred to a glucose batch culture for time T_1. These cells were then moved to an ethanol batch culture for time T_2. Here, we used the same definition for lag time (T_L) as in the maltose-glucose-maltose shift experiment[54]. Simulation results confirm that prolonging the period of growth in glucose lengthens the lag phase after the glucose-to-ethanol shift (Fig. 4b,c).

Next, we used our model to understand how additional time spent in glucose extends the lag phase. Upon the ethanol-to-glucose shift, the precursor and amino acid concentrations both increase significantly, causing the active SNF1 and TORC1 concentrations to quickly drop and rise, respectively (Supplementary Fig. 12). These changes in signaling promote the production of

R proteins to support fast growth on glucose. Concurrently, the drop in SNF1 activity represses the synthesis of E_{gn} and E_{mt}, both of which are essential for growth on ethanol. Although we do not consider active protein degradation, E_{gn} and E_{mt} are still lost through growth-induced dilution. Therefore, the longer the cells are exposed glucose, the lower their starting E_{gn} and E_{mt} concentrations are upon switching from glucose to ethanol (Supplementary Fig. 13a,b).

Importantly, we assumed that growth rate is proportional to the protein synthesis rate (Supplementary Method 1.6). Therefore, because amino acids and ATP are both inputs for the gene regulation module, growth rate resumption after the nutrient shift is ultimately determined by the time it takes for these metabolites to reaccumulate. E_{gn} and E_{mt} catalyze the conversions from ethanol to precursor to ATP. They play a significant role in determining ATP availability during growth on ethanol. Additionally, because amino acid uptake requires ATP, these enzymes also affect amino acid availability. Cells that have spent a long time growing in glucose require more time to reaccumulate E_{gn} and E_{mt} (Supplementary Fig. 13c,d) and, consequently, more time to reaccumulate ATP (Supplementary Fig. 13e) and amino acids (Supplementary Fig. 13f), i.e., their lag time is longer (Fig. 4c,e and Supplementary Fig. 13g,h).

Recent experiment results have shown that mutations of respiration-related genes, which are coarse-grained into E_{mt}, affect the lag phase length[54,55]. Specifically, deletions of genes within the electron transport chain lengthen the lag phase while overexpression of *HAP4*, a transcriptional activator for respiration-related genes, decreases lag[54,55]. To verify that our model reproduces this result, we modulated the value for the maximal level of transcriptional regulation by SNF1 on E_{mt} synthesis ($\xi_{mt,s}$) and investigated the effect on lag time. Consistent with experiment, the lag time decreases with increasing E_{mt} synthesis (Fig. 4g,h). E_{mt} catalyzes the production of ATP from precursor, the only source of ATP during ethanol utilization. Generation of ATP is required to fuel amino acid uptake and protein synthesis.

Differential growth in rich and minimal media. Cultivation media has a major effect on an organism's phenotype because nutrient quality impacts cellular resource allocation, which, in turn, dictates growth rate and chemical production[33,56,57]. To further understand the role that cultivation media plays, we investigated how cells grown in minimal media, which contains only essential nutrients, differ in their metabolic reactions, signaling, and gene regulation compared to cells grown in rich media, minimal media supplemented with additional amino acids[58,59]. Minimal

media is simulated by setting the extracellular amino acid concentration to zero whereas this concentration is set to a high, saturating value for rich media (Fig. 5a and Supplementary Method 4.4). Simulations of glucose batch experiments show that cells grown in rich media (Fig. 5, green lines and bars) deplete glucose faster (Fig. 5b), produce more ethanol (Fig. 5c), and grow faster (Fig. 5d) than cells grown in minimal media (Fig. 5c-d, blue lines), consistent with experiment data (Fig. 5e-g).

The difference in growth rate is caused by distinct responses in the signaling and gene regulation modules. In rich media, yeast uptakes amino acids instead of synthesizing them[60,61] (Supplementary Fig. 14a). Consequently, these cells have a higher intracellular amino acid concentration[62,63,64] (Supplementary Fig. 14b) and greater TORC1 activity (Supplementary Fig. 14c) than cells growth in minimal media. Because TORC1 channels resources away from the production of amino acid biosynthesis enzymes (E_{as}) and towards R protein synthesis (Fig. 5h,i), cells grown in rich media also have larger ribosome concentrations (Supplementary Fig. 14d). The concentrations of the other protein sectors are comparable for both media types (Supplementary Fig. 15). Cells grown in rich media also have a larger charged tRNA concentration due to their augmented intracellular amino acid concentration. The combination of both the increased ribosome and charged tRNA concentrations yields a greater concentration of translating ribosomes (Supplementary Fig. 14e) and, therefore, a faster growth rate.

The simulation shows that cells grown in rich media have a larger single-cell glucose uptake rate than cells cultivated with minimal media (Fig. 5j, left bars), which contrasts with experiment (Fig. 5k, left bars). This inconsistency is a limitation of our simplified model. The glucose-to-precursor reaction generates ATP (Fig. 1b) and is subject to feedback inhibition by ATP. Because the concentration of ATP is lower in cells grown in rich media (Supplementary Fig. 16a), this ATP inhibition is reduced, and the glucose uptake rate is larger. However, the increased glucose uptake rate contributes to a larger precursor concentration (Supplementary Fig. 16b). This increased substrate availability for the precursor-to-ethanol reaction facilitates the elevated ethanol production rate observed for these cells, which is consistent with experiment (Fig. 5j,k, right bars). Our model captures the phenotypic differences between cells grown in rich and minimal media downstream of precursor. The discrepancy in the glucose uptake rate lies upstream of precursor and will be resolved by expanding our model description for the glucose-to-precursor reaction.

Model modularity allows zooming in on specific pathways. With our coarse-grained, integrated framework, we were able to greatly simplify the complexity yet still capture the defining properties of *S. cerevisiae* metabolism. However, one major shortcoming of this one-precursor formulation is the lack metabolic detail. For example, enzymes for the glyoxylate cycle and gluconeogenesis were coarse-grained into E_{gn} because both pathways are essential for growth on ethanol. In reality, the glyoxylate cycle and gluconeogenesis are separate. Moreover, we lumped metabolic precursors and amino acids into effective molecules that represent the growth-limiting precursor and amino acid, whereas in cells, the twenty amino acids are derived from several distinct metabolic precursors. Here, we show that the modularity of our model allows us to easily expand and describe individual pathways for greater resolution. Although our aim is to increase model resolution, we still use coarse-graining to manage system complexity.

Here, we zoomed-in on our glucose-to-precursor reaction to illustrate how our model can be extended. Four changes were made for this expansion (Supplementary Method 3). (1) The singular precursor was divided into four precursors that each represent different groups of glycolytic intermediates (Fig. 6a, Supplementary Fig. 17, Supplementary Method 3.1.1). Specifically, precursors one and two describe upper glycolysis metabolites, and lower glycolysis metabolites are represented by precursors three and four. The forward flux from precursor one to precursor four represents glycolysis. Gluconeogenesis is the reverse flux from precursor four to precursor one. For simplicity, we assume that the same E_{gy} and E_{gn} enzymes catalyze the forward and reverse reactions, respectively. (2) Amino acid production requires precursor one, precursor three, and precursor four as substrates (Supplementary Method 3.1.3). (3) Precursor two, which plays a similar role to the glucose uptake flux sensor fructose-1,6-bisphosphate[31,32,65], inhibits SNF1 activity (Supplementary Method 3.2). (4) The one-precursor model E_{gy} enzyme was separated into two enzymes for glucose uptake and phosphorylation (E_{ht}) and glycolysis (E_{gy}) (Supplementary Methods 3.1.1 and 3.3). The one-precursor model E_{gn} enzyme was replaced by two enzymes for ethanol uptake and the glyoxylate cycle (E_{go}) and gluconeogenesis (E_{gn}).

Our four-precursor model captures the distinct trends exhibited by the upper and lower glycolysis metabolites in cells grown in both chemostat and batch experiments (Fig. 6b-i). Importantly, the results of our four-precursor model simulations are consistent with the results of our one-precursor model simulations while providing greater resolution of the underlying metabolites and protein abundances (Supplementary Figs. 18 and 19). This model extension also

allowed us to expand on our discussion of the origin of the diauxic lag (Supplementary Method 3.4 and Supplementary Figs. 20 and 21) and resolve the glucose uptake rate discrepancy identified in the one-precursor model simulations when comparing cell growth in rich and minimal media (Supplementary Methods 3.5 and Supplementary Figs. 22 and 23).

Discussion

Microbial metabolism is characterized by a remarkable degree of complexity and is distinguished by its emergent properties. In this study, we constructed a quantitative modeling framework of *S. cerevisiae* metabolism and used it to examine the molecular level coordination of carbon metabolism and the resultant collective cellular behaviors. The framework successfully captures the Crabtree effect and the diauxic shift and describes the molecular origin of the diauxic lag time. The model also demonstrates differential growth under nutrient-altered environments, and its construction enables more detailed elucidation of specific pathways of interest.

Underlying the framework are three key pillars, namely coarse graining, systems, and dynamics. Coarse graining allowed us to reduce complexity significantly while the systems and dynamic descriptions conferred explicit consideration of the coordination between metabolic reactions, signaling, and gene regulation and the temporal evolution of molecules and of the environment. This modeling approach allowed us to bear a manageable degree of model complexity to derive fundamental biophysical insights that are otherwise challenging to obtain. Our model is complementary to genome-scale and detailed kinetic models that focus on the comprehensive description of detailed processes.

The modularity of the framework offers a systematic path for further investigation of cellular metabolism. Being able to zoom in on specific metabolites or pathways by introducing detailed local reactions while keeping the rest coarse-grained will help us examine specific metabolic events in detail and design and optimize biosynthetic pathways in *S. cerevisiae* for chemical production. Additionally, the framework can be adapted to describe the metabolism of non-model yeasts, such as *Yarrowia lipolytica* and *Issatchenkia orientalis*. Together, this study advances the basic understanding of quantitative microbial physiology and provides insights into yeast metabolic engineering for biotechnological purposes.

Methods

General description. The modeling framework was developed by decomposing the system into three modules: metabolic reactions, signaling, and gene regulation. The modules were constructed and characterized individually and then reassembled into one cohesive framework. All simulations were implemented using custom MATLAB (MathWorks) codes. Mutations were implemented by altering the values of the corresponding parameters. The model was further extended from a one-precursor to a four-precursor description. See supplementary files for a detailed description of the model construction and extension, parameters, and computational methods.

Cell physiology and resource partition. The model involves cellular processes related to glucose, ethanol, metabolic precursors, amino acids, ATP, ribosomes, tRNA, proteins, SNF1, and TORC1. Proteins were classified into three types: cytosolic ribosomal and ribosome-affiliated proteins and other transcription and translation machinery (R sector), metabolic enzymes and plasma membrane nutrient transporters (E sector), and other proteins (Z sector). The E sector was further sub-divided into eight groups depending on the reactions they catalyzed: glucose uptake and catabolism (E_{gy}), respiration (E_{mt}), ethanol fermentation (E_{fe}), ethanol uptake and catabolism (E_{gn}), and amino acid biosynthesis (E_{as}) and uptake (E_{at}). A biophysical model for protein synthesis from amino acids was developed. Regulation of resource partitioning is incorporated through local feedback inhibition of precursor, amino acid, and ATP synthesis, regulation mediated by growth and dilution, and SNF1 and TORC1 regulation of protein expression and activity in response to the extracellular glucose and intracellular amino acid concentrations. The transient growth rate is assumed to be proportional to the total protein synthesis rate of the cell.

Data acquisition and processing. Time courses were simulated by numerically solving the differential equations of the model.

Data availability. The data that support the conclusions of this study are available from the corresponding author upon request.

Code availability. The source codes for the model are available from the corresponding author upon request at http://lulab.bioen.illinois.edu/links.html.

References

1. Ramirez-Gaona, M. et al. YMDB 2.0: a significantly expanded version of the yeast metabolome database. Nucleic Acids Res. **45**, 440–445 (2017).
2. Santangelo, G. M. Glucose signaling in Saccharomyces cerevisiae. *Microbiol. Mol. Biol. Rev*. **70**, 253–282 (2006).
3. Conrad, M. et al. Nutrient sensing and signaling in the yeast *Saccharomyces cerevisiae*. *FEMS Microbiol. Rev*. **38**, 254–299 (2014).
4. Zaman, S., Lippman, S. I., Zhao, X. & Broach, J. R. How *Saccharomyces* responds to nutrients. *Annu. Rev. Genet*. **42**, 27–81 (2008).
5. Broach, J. R. Nutritional control of growth and development in yeast. *Genetics* **192**, 73–105 (2012).
6. Ljungdahl, P. O. & Daignan-Fornier, B. Regulation of amino acid, nucleotide, and phosphate metabolism in *Saccharomyces cerevisiae*. *Genetics* **190**, 885–929 (2012).
7. Hoek, P. V., Dijken, J. P. V. & Pronk, J. T. Effect of specific growth rate on fermentative capacity of baker's yeast. *Appl. Environ. Microbiol*. **64**, 4226–4233 (1998).
8. DeRisi, J. L., Iyer, V. R. & Brown, P. O. Exploring the metabolic and genetic control of gene expression on a genomic scale. *Science* **278**, 680–686 (1997).
9. Zampar, G. G. et al. Temporal system-level organization of the switch from glycolytic to gluconeogenic operation in yeast. *Mol. Syst. Biol*. **9**, 651 (2013).
10. Murphy, J. P., Stepanova, E., Everley, R. A., Paulo, J. A., & Gygi, S. P. Comprehensive temporal protein dynamics during the diauxic shift in *Saccharomyces cerevisiae*. *Mol. Cell. Proteomics*, **14**, 2454-2465 (2015).
11. Parapouli, M., Vasileiadis, A., Afendra, A. S. & Hatziloukas, E. *Saccharomyces cerevisiae* and its industrial applications. *AIMS microbiology*, **6**, 1-31 (2020).
12. Nielsen, J., Larsson, C., van Maris, A. & Pronk, J. Metabolic engineering of yeast for production of fuels and chemicals. *Curr. Opin. Biotechnol*. **24**, 398–404 (2013).
13. Karathia, H., Vilaprinyo, E., Sorribas, A. & Alves, R. Saccharomyces cerevisiae as a model organism: A comparative study. PLoS ONE **6**, (2011).

14. Tenreiro, S., Franssens, V., Winderickx, J. & Outeiro, T. F. Yeast models of Parkinson's disease-associated molecular pathologies. *Curr. Opin. In Gene. & Dev.*, **44**, 74–83 (2017).
15. Tenreiro, S. & Outeiro, T. F. Simple is good: Yeast models of neurodegeneration. FEMS Yeast Research **10**, 970–979 (2010).
16. Thines, L., Deschamps, A., Stribny, J. & Morsomme, P. Yeast as a tool for deeper understanding of human manganese-related diseases. Genes **10**, (2019).
17. Menacho-márquez, M. & Murguía, J. R. Yeast on drugs: Saccharomyces cerevisiae as a tool for anticancer drug research. *Clin. Transl. Oncol*. **9**, 221–228 (2007).
18. Kesten, D., Kummer, U., Sahle, S. & Hübner, K. A new model for the aerobic metabolism of yeast allows the detailed analysis of the metabolic regulation during glucose pulse. *Biophysical chemistry*, **206**, 40–57 (2015).
19. Teusink, B. et al. Can yeast glycolysis be understood in terms of in vitro kinetics of the constituent enzymes? Testing biochemistry. *Eur. J. Biochem*. **267**, 5313–5329 (2000).
20. van Eunen, K., Kiewiet, J. A., Westerhoff, H. V. & Bakker, B. M. Testing biochemistry revisited: how in vivo metabolism can be understood from in vitro enzyme kinetics. *PloS Comput. Biol*. **8**, e1002483 (2012).
21. Lei, F., Rotbøll, M. & Jørgensen, S. B. A biochemically structured model for *Saccharomyces cerevisiae*. *J. Biotechnol*. **88**, 205–221 (2001).
22. Förster, J., Famili, I., Fu, P., Palsson, B., & Nielsen, J. (2003). Genome-scale reconstruction of the Saccharomyces cerevisiae metabolic network. Genome Research, **13**, 244–253.
23. Heavner, B. D. & Price, N. D. Comparative Analysis of Yeast Metabolic Network Models Highlights Progress, Opportunities for Metabolic Reconstruction. PloS Computational Biology **11**, (2015).
24. Lu, H. et al. A consensus *S. cerevisiae* metabolic model Yeast8 and its ecosystem for comprehensively probing cellular metabolism. *Nat. Commun*. **10**, 3586 (2019).
25. Lao-Martil, D. et al. Kinetic modeling of *Saccharomyces cerevisiae* central carbon metabolism: achievements, limitations, and opportunities. *Metabolites*, **12,** 74 (2022).
26. Doan, D. T., Hoang, M. D., Heins, A. L. & Kremling, A. Applications of Coarse-Grained Models in Metabolic Engineering. *Front. Mol. Biosci*. **9**. 806213 (2022).

27. Solis-Escalante, D. et al. A minimal set of glycolytic genes reveals strong redundancies in Saccharomyces cerevisiae central metabolism. *Eukaryot. Cell* **14**, 804–816 (2015).
28. Tripodi, F., Nicastro, R., Reghellin, V. & Coccetti, P. Post-translational modifications on yeast carbon metabolism: regulatory mechanisms beyond transcriptional control. *Biochim. Biophys. Acta* **1850**, 620–627 (2015).
29. Dihazi, H., Kessler, R. & Eschrich, K. Glucose-induced stimulation of the Ras-cAMP pathway in yeast leads to multiple phosphorylations and activation of 6-phosphofructo-2-kinase. Biochemistry 42, 6275–6282 (2003).
30. Shirra, M.K. et al. A chemical genomics study identifies Snf1 as a repressor of GCN4 translation. *J. Biol. Chem*. **283**, 35889–35898 (2008).
31. Peeters, K. et al. Fructose-1,6-bisphosphate couples glycolytic flux to activation of Ras. *Nat. Commun.* **8**, 922 (2017).
32. Milanesi, R., Tripodi, F., Vertemara, J., Tisi, R. & Coccetti, P. AMPK Phosphorylation Is Controlled by Glucose Transport Rate in a PKA-Independent Manner. *Int J Mol Sci*. **22**, 9483 (2021).
33. Scott, M., Gunderson, C. W., Mateescu, E. M., Zhang, Z. & Hwa, T. Interdependence of cell growth and gene expression: origins and consequences. *Science* **330**, 1099–1102 (2010).
34. Liao, C., Blanchard, A. E. & Lu, T. An integrative circuit-host modelling framework for predicting synthetic gene network behaviours. *Nat. Microbiol*. **2**, 1658–1666 (2017).
35. Kayikci, O. & Nielsen, J. Glucose repression in *Saccharomyces cerevisiae*. *FEMS Yeast Res*. **15**, fov068 (2015).
36. Bianchi, F., van't Klooster, J. S., Ruiz, S. J. & Poolman, B. Regulation of amino acid transport in *Saccharomyces cerevisiae*. *Microbiol. Mol. Biol. Rev.* **83**, e00024-19. (2019).
37. Kumar, K., Venkatraman, V. & Bruheim, P. Adaptation of central metabolite pools to variations in growth rate and cultivation conditions in Saccharomyces cerevisiae. *Microbial Cell Factories* **20** (2021).
38. Hackett, S. R. et al. Systems-level analysis of mechanisms regulating yeast metabolic flux. *Science* **354** (2016).

39. Boer, V. M., Crutchfield, C. A., Bradley, P. H., Botstein, D. & Rabinowitz, J. D. Growth-limiting intracellular metabolites in yeast growing under diverse nutrient limitations. *Molecular Biology of the Cell* **21**, 198–211 (2010).
40. Xia, J., Sánchez, B.J., Chen, Y. *et al.* Proteome allocations change linearly with the specific growth rate of *Saccharomyces cerevisiae* under glucose limitation. *Nat Commun* **13,** 2819 (2022).
41. Famili, I., Forster, J., Nielsen, J. & Palsson, B. O. *Saccharomyces cerevisiae* phenotypes can be predicted by using constraint-based analysis of a genome-scale reconstructed metabolic network. *Proc. Natl Acad. Sci.* **100**, 13134–13139 (2003).
42. Nilsson, A. & Nielsen, J. Metabolic trade-offs in yeast are caused by F1F0-ATP synthase. *Sci. Rep*. **6**, 22264 (2016).
43. Sánchez, B. J. et al. Improving the phenotype predictions of a yeast genome-scale metabolic model by incorporating enzymatic constraints. *Mol. Syst. Biol.* **13**, 935 (2017).
44. de Groot, D. H., et al. The common message of constraint-based optimization approaches: overflow metabolism is caused by two growth-limiting constraints. *Cell. Mol. Life Sci*. **77**, 441–453 (2020).
45. Niebel, B., Leupold, S. & Heinemann, M. An upper limit on Gibbs energy dissipation governs cellular metabolism. *Nat. Metab*. **1**, 125–132 (2019).
46. Molenaar, D., van Berlo, R., de Ridder, D. & Teusink, B. Shifts in growth strategies reflect tradeoffs in cellular economics. *Mol. Syst. Biol*. **5**, 323 (2009).
47. Basan, M. et al. Overflow metabolism in *Escherichia coli* results from efficient proteome allocation. *Nature* **528**, 99–104 (2015).
48. Suarez-Mendez, C. et al. Interaction of storage carbohydrates and other cyclic fluxes with central metabolism: A quantitative approach by non-stationary 13C metabolic flux analysis. *Metab. Eng. Commun*. **3**, 52–63 (2016).
49. Huberts, D. H., Niebel, B. & Heinemann, M. A flux-sensing mechanism could regulate the switch between respiration and fermentation. *FEMS Yeast Res*. **12**, 118–128 (2012).

549 50. Bosch, D., Johansson. et al. Characterization of glucose transport mutants of
550 *Saccharomyces cerevisia*e during a nutritional upshift reveals a correlation between
551 metabolite levels and glycolytic flux. *FEMS Yeast Res*. **8** 10-25 (2008).
552 51. Bradley, P. H., Brauer, M. J., Rabinowitz, J. D. & Troyanskaya, O. G. Coordinated
553 Concentration Changes of Transcripts and Metabolites in *Saccharomyces cerevisiae*.
554 *PLOS Comput. Biol*. **5**, e1000270 (2009).
555 52. Di Bartolomeo, F. et al. Absolute yeast mitochondrial proteome quantification reveals
556 trade-off between biosynthesis and energy generation during diauxic shift. *Proc. Natl*
557 *Acad. Sci.* **117**, 7524-7535 (2020).
558 53. Vermeersch, L. et al. On the duration of the microbial lag phase. *Curr. Genet*. **65**, 1–7
559 (2019).
560 54. Cerulus, B. et al. Transition between fermentation and respiration determines
561 history-dependent behavior in fluctuating carbon sources. *eLife* **7**, e39234 (2018).
562 55. Perez-Samper, G. et al. The crabtree effect shapes the Saccharomyces cerevisiae lag
563 phase during the switch between different carbon sources. mBio 9, e01331–18
564 (2018).
565 56. Tibocha-Bonilla, J. D. et al. Dynamic resource allocation drives growth under nitrogen
566 starvation in eukaryotes. *npj Syst. Biol. Appl*. **6**, 14 (2020).
567 57. Hahn-Hagerdal, B. et al. Role of cultivation media in the development of yeast strains
568 for large scale industrial use. *Microb. Cell Fact.* **4**, 31 (2005).
569 58. Björkeroth, J. et al. Proteome reallocation from amino acid biosynthesis to ribosomes
570 enables yeast to grow faster in rich media. *Proc. Natl Acad. Sci*. **117**, 21804–21812
571 (2020).
572 59. Kim, J. & Kim, K. H. Effects of minimal media vs. complex media on the metabolite
573 profiles of *Escherichia coli* and *Saccharomyces cerevisiae*. *Process Biochem.* **57**, 64-71.
574 (2017).
575 60. Kevvai, K., Kütt, M. L., Nisamedtinov, I. & Paalme, T. Simultaneous utilization of
576 ammonia, free amino acids and peptides during fermentative growth of
577 *Saccharomyces cerevisiae*. *J. Inst. Brew*. 122, 110-115 (2016).

61. Zhang, W., Du, G., Zhou, J. & Chen, J. Regulation of Sensing, Transportation, and Catabolism of Nitrogen Sources in Saccharomyces cerevisiae. *Microbiology and Molecular Biology Reviews* **82**, (2018).
62. Kitamoto, K., Yoshizawa, K., Ohsumi, Y. & Anraku, Y. Dynamic aspects of vacuolar and cytosolic amino acid pools of *Saccharomyces cerevisiae*. *J. Bacteriol*. **170**, 2683–2686 (1988).
63. Martíez-force, E. & Benítez, T. Changes in yeast amino acid pool with respiratory versus fermentative metabolism. *Biotechnol. Bioeng*. **40**, 643-649 (1992).
64. Martinez-Force, E. & Benitez, T. Effects of varying media, temperature, and growth rates on the intracellular concentrations of yeast amino acids. *Biotechnol. Prog*. **11**, 386–392 (1995).
65. Lemus, M. R. et al. The role of glycolysis-derived hexose phosphates in the induction of the Crabtree effect. *JBC*. **293**, 12843-12854 (2018).

Acknowledgements

This work was supported by the DOE Center for Advanced Bioenergy and Bioproducts Innovation (U.S. Department of Energy, Office of Science, Office of Biological and Environmental Research under Award Number DE-SC0018420) and the National Institute of General Medical Sciences (GM133579). Any opinions, findings, and conclusions or recommendations expressed in this publication are those of the author(s) and do not necessarily reflect the views of the U.S. Department of Energy.

Author contributions

T. L. conceived and directed the study and designed the research. V.N. and Y.L. contributed to model development. V.N and Y.L. analyzed data. V.N. and T.L. wrote the paper. All authors discussed the results and commented on the manuscript.

Additional information

Supplementary information is available for this paper.

Correspondence and requests for materials should be addressed to T. L.

Competing interests

The authors declare no competing financial interests.

Figures

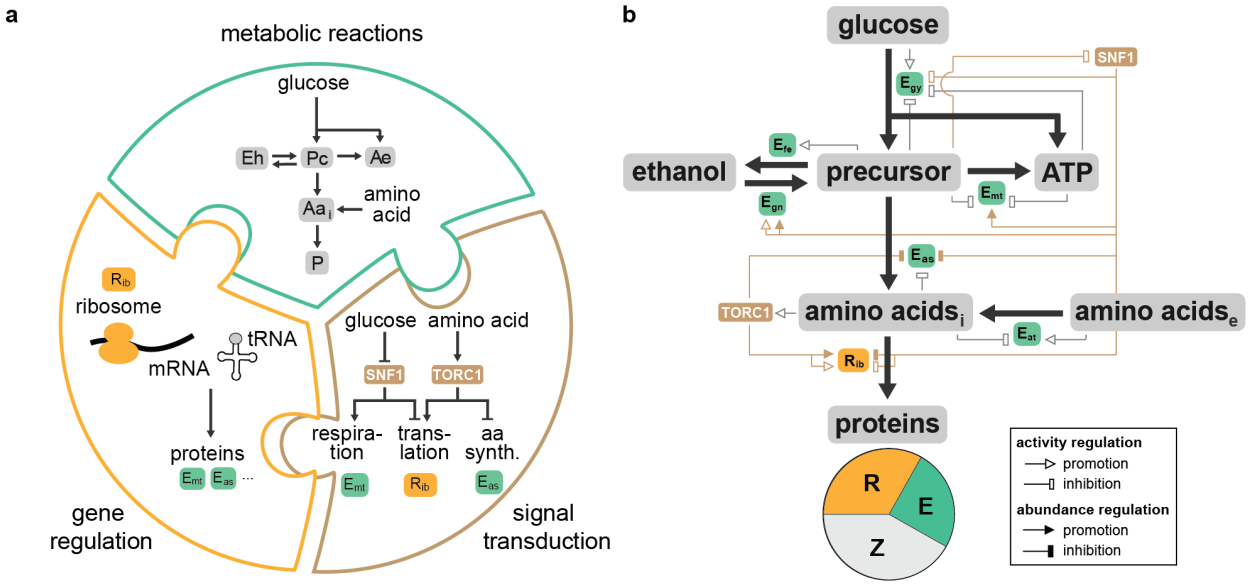

Figure 1 | A systems view of the metabolic reactions, signaling, and gene regulation of *S. cerevisiae*. **A**, Schematic illustration of *S. cerevisiae* metabolism, which involves the orchestration of metabolic, signaling, and gene regulation networks. **B**, Coarse-grained model of *S. cerevisiae* metabolism. Metabolic reactions for carbon conversion are coarse-grained. Here, glucose is converted to a precursor that is subsequently used to produce ethanol, amino acids, and ATP. Ethanol can also be consumed to produce the precursor for successive conversion. In addition to de novo synthesis, amino acids can be directly acquired from the environment through uptake. Meanwhile, amino acids are used to synthesize proteins and enable cellular growth. The proteome is coarse-grained into three sectors, namely ribosomal and ribosome-affiliated proteins €, nutrient transporters and metabolic proteins €, and housekeeping proteins (Z). The E sector is further divided into six subsectors, including enzymes for glucose utilization (E_{gy}), fermentation (E_{fe}), respiration (E_{mt}), amino acid biosynthesis (E_{as}) and uptake (E_{at}), and ethanol utilization (E_{gn}). Additionally, coarse-grained signaling pathways centered around SNF1 and TORC1 sense the abundances of glucose and intracellular amino acids. These signaling molecules regulate both the activity and abundance of proteins to achieve a coordinated and dynamic cellular metabolism.

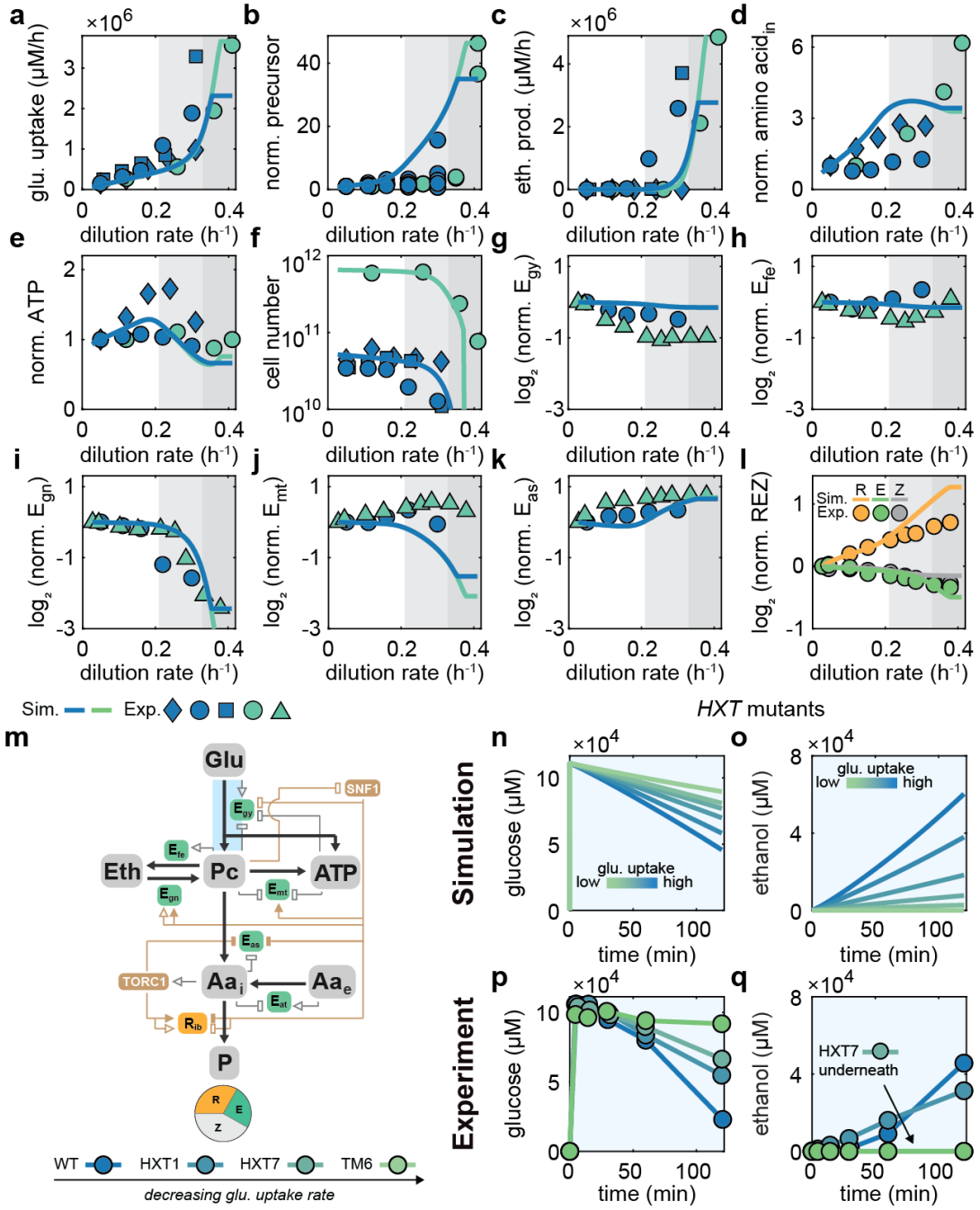

Figure 2 | The Crabtree effect and critical dilution rate of *S. cerevisiae*. A-l, Comparison of simulation (lines) with experiment[37-40] (circles, squares, diamonds, and triangles) of wild type cells grown in glucose-limited chemostats with no extracellular amino acids: **a**, glucose uptake rate, **b**, precursor, **c**, ethanol production rate, **d,** intracellular amino acids, **e**, ATP, **f**, cell number, and **g-l**, proteins as a function of dilution rate. Different colored lines represent simulations with different glucose feed concentrations. Green: 10 g/L, blue: 0.8 g/L. The precursor concentration

637 is normalized to its value at the final and the amino acid, ATP, and protein concentrations are
638 normalized to their values at the first simulated or experimentally measured dilution rates. The
639 background color indicates the cell's type of metabolism. White: purely oxidative, dark gray:
640 respire-fermentative. The light gray background highlights the range of experimentally measured
641 critical dilution rates from refs. 37 and 38. **m-q**, Decreasing the glucose uptake rate reduces
642 overflow metabolism. **m**, Schematic diagram highlighting the location of HXT proteins in the
643 model. **n-q**, Comparison of the simulated (**n**,**o**) and experimentally measured[50] (**p**,**q**) glucose and
644 ethanol profiles during a glucose pulse experiment with no extracellular amino acids of the wild
645 type and hexose transporter mutants with high (HXT1), intermediate (HXT7) and low (TM6)
646 glucose uptake rates. Details for the experiment data can be found in Supplementary Table 3.
647 Simulation details are in Supplementary Methods 4.1.
648

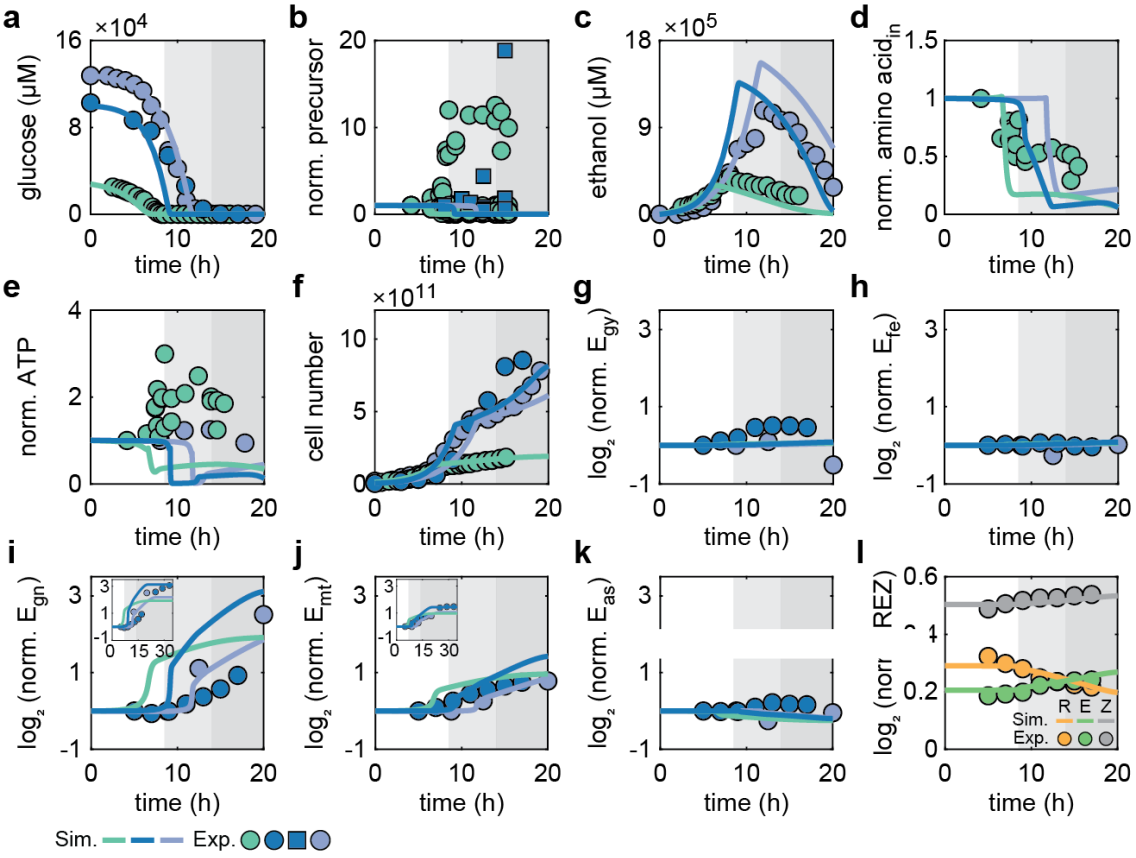

Figure 3 | Diauxic growth of *S. cerevisiae* in glucose batch fermentations. a-l, Comparison of simulation (lines) with experiment (circles) for wild type cells grown in glucose batch experiments: **a-e**, metabolites, **f**, cell number, and **g-l**, proteins as functions of time. Different colored lines represent simulations with different initial conditions. Green: 5 g/L glucose with no extracellular amino acids, blue: 18 g/L glucose with a saturating concentration of extracellular amino acids, purple: 23 g/L glucose with no extracellular amino acids. The precursor, intracellular amino acid, and ATP concentrations are normalized to their values at the first simulated or experimentally measured values. The insets in panels **i** and **j** show the entire time course for the blue simulation and experiment. The background color indicates the cellular metabolism corresponding to the available carbon source. White: glucose consumption, dark gray: ethanol consumption. The light gray background highlights the range of experimentally measured glucose depletion times from refs. 9, 10, and 52. Details for the experiment data can be found in Supplementary Table 3. Simulation details are in Supplementary Methods 4.2.

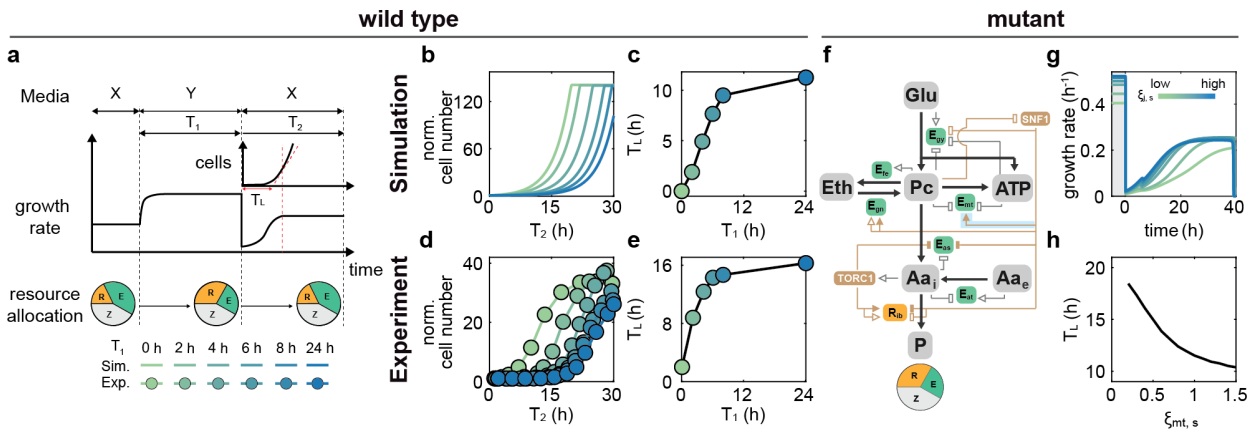

Figure 4 | Origin of diauxic lag time from cellular resource re-allocation. a, Illustration of the ethanol-glucose-ethanol shift experiment. Cultures adapted to growth on ethanol (media X) are transferred to glucose (media Y) for varying amounts of time T_1 (0, 2, 4, 6, 8, or 24 hours). Cells are then transferred back to ethanol for time T_2 and experience a lag phase (T_L) before resuming growth. **b**,**c**, Simulated lag time after an ethanol-glucose-ethanol shift for wild type cells. **d**,**e**, Experimentally measured[54] lag time after a maltose-glucose-maltose shift for wild type cells. Different colors of lines indicate different lengths of time spent in glucose (T_1). The simulation results for the ethanol-glucose-ethanol shift are qualitatively consistent with the experiment data for the maltose-glucose-maltose shift. **f-h**, Mutations affecting respiration alter the lag time length. **f**, Respiratory mutants were modeled by perturbing the value of the maximum level of transcriptional regulation by SNF1 on E_{mt} synthesis ($\xi_{mt,s}$). Different colors of lines indicate different $\xi_{mt,s}$ values used for the simulation. **g**,**h**, Growth rate (**g**) and lag time (**h**) of simulated respiratory mutants. Details for the experiment data can be found in Supplementary Table 3. Simulation details are in Supplementary Methods 4.3.

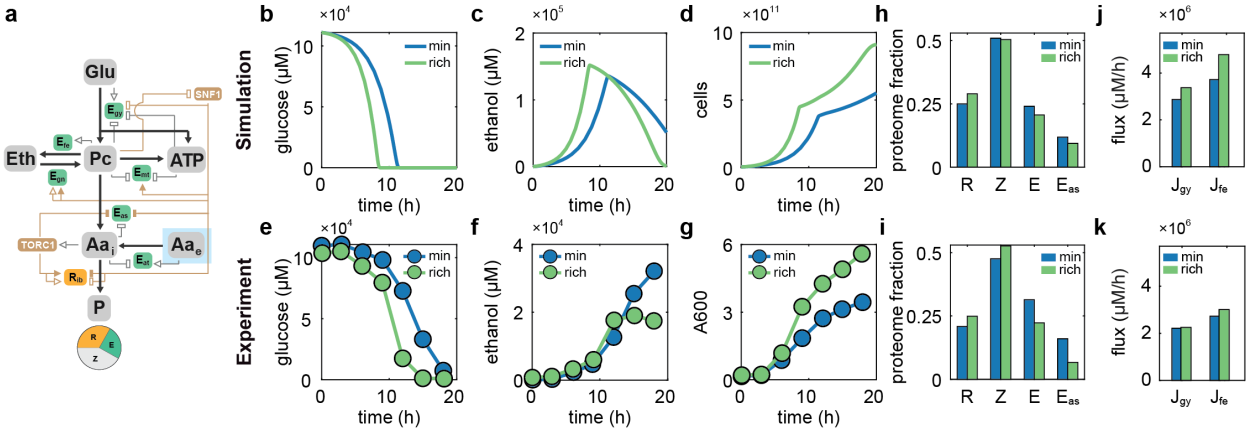

Figure 5 | Different growth phenotypes in minimal and rich media. a, Rich media differs from minimal media by the addition of extracellular amino acids. The extracellular amino acid concentration was set to zero for minimal media or to a high, saturating value for rich media. **b-k**, Comparison of simulation (**b-d**,**h**,**j**) with experiment[58,59] (**d**,**e**,**g**,**i**) of wild-type cells during exponential growth in glucose batch cultures with minimal (blue) or rich (green) media: glucose (**b**,**e**), ethanol (**c**,**f**), and cell growth (**d**,**g**) profiles; R, E, Z, and E_{as} protein fractions (**h**,**i**); and single-cell glucose uptake and ethanol production rates (**j**,**k**). Details for the experiment data can be found in Supplementary Table 3. Simulation details are in Supplementary Methods 4.4.

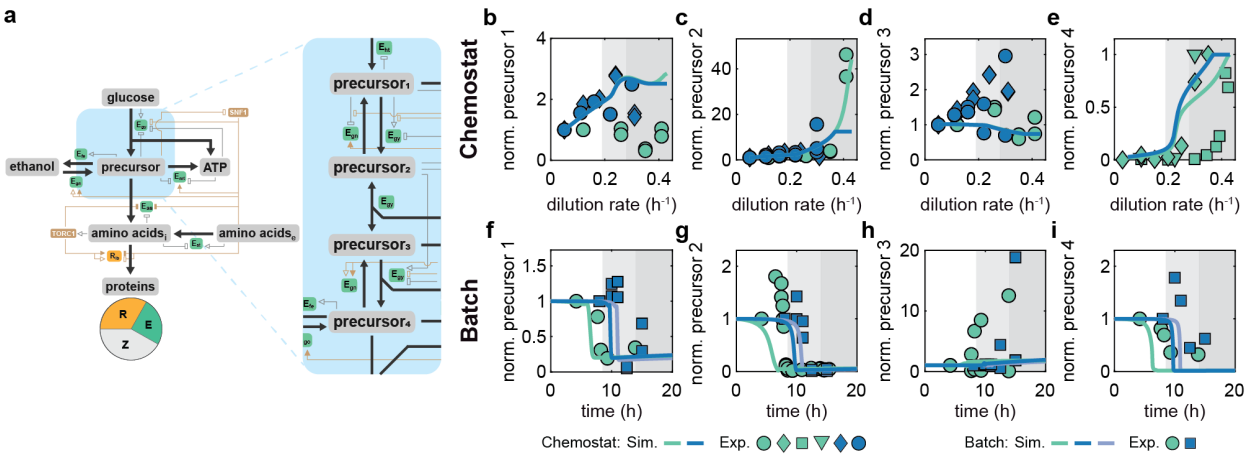

Figure 6 | Model expansion to a four-precursor description for detailed glycolysis analysis. **a**, Extension of our one-precursor model to a four-precursor description. The singular precursor was divided into four separate precursors. Upper glycolysis metabolites are represented by precursors one and two. Lower glycolysis metabolites are described by precursors three and four. **b-i**, Comparison of simulation (lines) with experiment (circles, squares, diamonds, and triangles) of the four precursor concentrations for cells grown in glucose-limited chemostats experiments (**b-e**) and glucose batch fermentations (**f-i**). Different colored lines and symbols represent different initial conditions. For the chemostat plots. Green: 10 g/L glucose and no extracellular amino acids, blue: 0.8 g/L glucose and no extracellular amino acids. For the batch plots, green: 5 g/L glucose and no extracellular amino acids, blue: 18 g/L glucose with a saturating concentration of extracellular amino acids, purple: 23 g/L glucose and no extracellular amino acids. Details for the experiment data can be found in Supplementary Table 3. Simulation details are in Supplementary Methods 4.5.